ELSEVIER

Materials Science and Engineering B 148 (2008) 154–161

MATERIALS SCIENCE & ENGINEERING B

www.elsevier.com/locate/mseb

# Dependence of photocatalytic activity on the compositions and photo-absorption of functional $TiO_2$–$Fe_3O_4$ coatings deposited by plasma spray

F.X. Ye [a,*], T. Tsumura [b], K. Nakata [b], A. Ohmori [c]

[a] *School of Materials Science & Engineering, Tianjin University, Weijin Road No. 92, Tianjin 300072, PR China*
[b] *Joining and Welding Research Institute, Osaka University, Osaka, Japan*
[c] *Tocalo Co. Ltd., Minamifutami, Futami-Cho, Akashi, Japan*

Received 28 May 2007; received in revised form 11 August 2007; accepted 3 September 2007

**Abstract**

Owing to the much concern with global environmental issues, $Fe_3O_4$ added photocatalytic $TiO_2$ coatings were deposited using plasma spray for environmental depollution. The influence of the content of $Fe_3O_4$ additive to the $TiO_2$ powder on the phase composition, microstructure and photo-absorption of plasma-sprayed $TiO_2$ coatings was systematically studied. The results showed that the $TiO_2$–$Fe_3O_4$ coatings consisted of anatase $TiO_2$, rutile $TiO_2$ and $Fe_2TiO_5$ pseudobrookite phase which appeared when the content of $Fe_3O_4$ additive was equal to or over 10%. The content of $FeTiO_3$ was highest in the sprayed $TiO_2$–10%$Fe_3O_4$ coatings. The addition of $Fe_3O_4$ improved the anatase–rutile transformation of $TiO_2$–$Fe_3O_4$ powders. Furthermore, it was found that $TiO_2$ coatings can decompose acetaldehyde under the illumination of ultraviolet rays, and the degrading efficiency was improved with an increase of $FeTiO_3$ content in the coatings. A two-step electron transfer model was proposed to explain the good photocatalytic activity of the sprayed coating with high content of $FeTiO_3$. However, presence of large amount of $Fe_2TiO_5$ compound substantially reduced the photocatalytic efficiency of the sprayed $TiO_2$–$Fe_3O_4$ coatings for its unfavorable photo-excited electron–hole transfer process.


*Keywords:* Plasma spray; Titanium dioxide; Iron oxide; Ilmenite; Photocatalytic; Photo-absorption

## 1. Introduction

To solve the environmental problems related to the hazardous wastes, contaminated groundwater and toxic air contaminants, extensive research is underway to develop commercial photocatalysts, which involve in $TiO_2$, CdS, $SnO_2$, $WO_3$, $SiO_2$, $ZrO_2$, ZnO, $Nb_2O_5$, $Fe_2O_3$, $SrTiO_3$, etc. [1–11]. Among all the oxide semiconductors that have been reported, titanium dioxide is an excellent photocatalyst due to its optical and electronic properties, chemical stability, non-toxicity and low cost [12–17].

However, it has been also realized that the band gap of anatase $TiO_2$ (about 3.2 eV) means that the electron can only be excited from the valence to the conduction band by the high power UV light irradiation with a wavelength shorter than 387 nm. This limits the application of sunlight as an energy source for the photocatalysis. Recently, visible light responsive photocatalysts are studied intensively. Domen have concentrated on the visible sensitized photocatalyst to splitting water by loading Pt, NiO, dyes on $TiO_2$ and by the other kind of photocatalyst such as $NaTaO_3$, $RuO_2$–loaded $Ge_3N_4$, etc [18–20]. Kudo reported the chromium and either tantalum or niobium–codoped $SrTiO_3$ photocatalyst with visible light response [21]. Asahi et al. reported the visible light photocatalysis in nitrogen-doped $TiO_2$ [22]. Anpo have synthesized iron ion-doped anatase $TiO_2$ by the hydrothermal method from titanium (IV) tetra-*tert*-butoxide and $FeCl_3$ or $FeCl_2$ solution [23] .The amount of doped iron ion plays a significant role in affecting its photocatalytic activity, and iron doped with optimum content can enhance photocatalytic activity, especially under visible light irradiation. Anpo also reported that the Fe ion-implanted $TiO_2$ catalysts enable the absorption of visible light up to a wavelength of 400–600 nm [24]. Some researcher also added the other semiconductors such as $WO_3$, $Al_2O_3$ into $TiO_2$ and fabricated composites to improve the photocatalytic activity of $TiO_2$ [6–11].

* Corresponding author. Tel.: +86 22 27406261; fax: +86 22 27404724.
*E-mail address:* yefx@tju.edu.cn (F.X. Ye).

0921-5107/$ – see front matter © 2007 Elsevier B.V. All rights reserved.
doi:10.1016/j.mseb.2007.09.057

Recently, plasma-spraying technique is widely applied to fabricate coating using feedstock powders such as $ZrO_2$, $Al_2O_3$ and $TiO_2$ to improve surface wear resistance. The coating formation speed is very high and it is easy to form composite coatings. A plasma-sprayed coating is formed by a stream of molten or half molten droplets impacting on the substrate followed by flattening, rapid solidification and cooling processes. The individual molten droplets spread to thin lamellae, the stacking of which constitutes the coating [25].

In this study, the $TiO_2$ and $TiO_2$–$Fe_3O_4$ coatings were deposited on stainless steel (JIS SUS304) by plasma-spraying technique, and effects of $Fe_3O_4$ content in the $TiO_2$–$Fe_3O_4$ feedstock powders on the phase composition and photocatalytic activity of the $TiO_2$ coatings were analyzed with scanning electron microscopy (SEM), energy dispersive analysis of X-ray (EDAX), X-ray diffraction (XRD), UV-3100PC scanning spectrophotometer and photocatalytic efficiency evaluation system in detail.

## 2. Materials and experimental procedures

### 2.1. Feedstock powders and substrate

To study the effects of $Fe_3O_4$ particles on the photocatalytic activity of $TiO_2$–$Fe_3O_4$ coatings in detail, five kinds of composite powders were designed, these were $TiO_2$–5 wt.%$Fe_3O_4$, $TiO_2$–10 wt.%$Fe_3O_4$, $TiO_2$–12.7 wt.%$Fe_3O_4$, $TiO_2$–22.5 wt.%$Fe_3O_4$ and $TiO_2$–32.6 wt.%$Fe_3O_4$ powders. The average sizes of $TiO_2$ and $TiO_2$–$Fe_3O_4$ powders were about 32 μm. The morphology of $TiO_2$ powder was spherical shape, which was very similar with that of $TiO_2$–$Fe_3O_4$ powders. It is very clear that the $Fe_3O_4$ additive was distributed uniformly in the agglomerated powder according to the EDAX maps. The substrate was stainless steel (JIS SUS304).

### 2.2. Coatings preparation and heat treatment of feedstock powders

The thermal spraying equipment was a plasma-spraying system (Plasmadyne-Mach1 manufactured by Plasmadyne Company). Argon was used as a primary plasma gas and helium was used as the secondary gas. The argon gas pressure and flow were 0.42 MPa and 58 slpm, respectively. The helium gas pressure and flow were 0.21 MPa and 9 slpm, respectively. The spraying distance was 70 mm. The arc voltage was 28–30 V. Except the specimen preparation to study the phase changes of $TiO_2$–32.6%$Fe_3O_4$ coating after heat treatment, which arc current of 600 A was chosen, arc current of 400 A was applied.

The anatase–rutile transformation temperature of pure anatase $TiO_2$ powder was approximate to 1173 K. To investigate the influence of the additive on the anatase–rutile phase transformation temperature and compare the composition variations of feedstock powders in heat treatment process and in thermal spray process, they were kept in electric furnace for 2 h after reaching at treated temperature (973 K, 1123 K, 1273 K or 1423 K) with a heating rate of 0.167 K/s, and then were cooled with the furnace.

### 2.3. Analysis of the feedstock powders and sprayed coatings

Scanning electron microscopy (SEM) and energy dispersive analysis of X-ray (EDAX) were used to examine the structure characteristics of the feedstock powders and the sprayed coatings. The phase composition of the heat-treated powders and the sprayed coatings was investigated by X-ray diffraction using Cu Kα radiation (λ = 1.5406 Å) and graphite crystal monochromator (JDX3530, JEOL, Japan). The $2\theta$ range was 23–38° including the main diffraction line of the possible phase compositions.

### 2.4. Diffuse reflectance spectroscopy and calculation of energy absorbance

The UV–VIS–NIR spectra of the feedstock powders and plasma-sprayed coatings were recorded using a Shimadzu UV-3100PC scanning spectrophotometer equipped with a diffuse reflectance accessory. The absorption intensity was calculated from the Kubelka–Munk equation as $f(R) = (1 - R)^2/2R$, where $f(R)$ is Kubelka–Munk value and $R$ is diffuse reflection of the powder or coating. The integrated energy absorbance from the light source of the sprayed coatings was estimated according to the following equation:

$$E_{\text{total}} = \int E(\lambda) f(R_\lambda)\, \mathrm{d}\lambda \quad (1)$$

where $E(\lambda)$ is the spectral irradiance of the light source, $f(R_\lambda)$ the Kubelka–Munk value and $E_{\text{total}}$ is the relative integrated energy absorbance. Generally, the increasing of $E_{\text{total}}$ benefits to increase the photocatalytic activity [26].

The study of the tail of the absorption curve of semiconductor shows that it has a simple exponential increase. The onset of this increase (point A in Fig. 1) has been suggested as a universal method of deducing the position of the absorption edge [27,28]. In this study, the wavelength coordinate of the point on

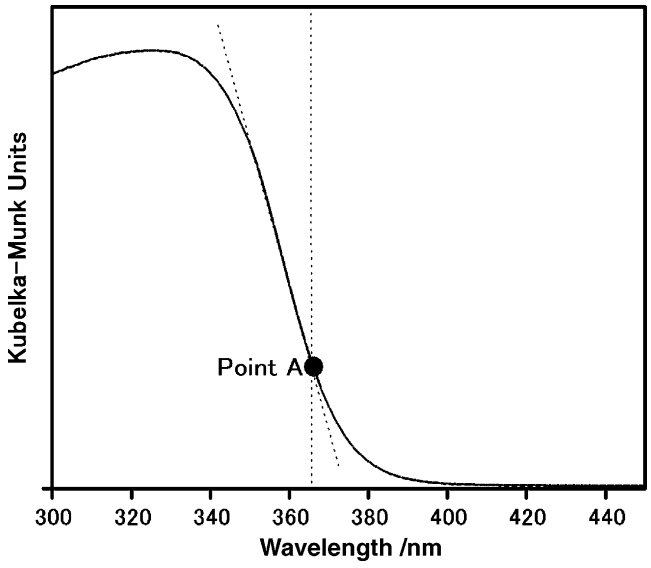


Fig. 1. Definition of absorption edge in absorption spectrum of semiconductor.

the low wavelength side of the curve at which the liner increase in absorbance starts was marked to investigate the absorption shift of feedstock powders and sprayed coatings.

### 2.5. Evaluation method of photocatalytic activity

In this experiment, the photocatalytic activity of the sprayed coatings was evaluated through the photo-decomposition of acetaldehyde. Fujishima reported the acetaldehyde is finally decomposed to $CO_2$ and $H_2O$ by $TiO_2$ photocatalyst [29]. The ultraviolet light (peak wavelength was 352 nm) intensity on the sample surface was set in 1.0 mW/cm$^2$. In the experimental procedure, the concentration (ppm) of the foul gas with time (s) was measured with a Kitakawa type gas detector at a certain time interval.

The results for photocatalytic efficiency of titanium dioxide indicated that the destruction rates of various contaminants by photocatalyst fit the Langmuir–Hinshelwood kinetic equation [30,31]. Langmuir–Hinshelwood explains the kinetics of heterogeneous catalytic processes and Langmuir adsorption isotherm is valid for the surface reaction. It is a first order kinetic equation. The Langmuir–Hinshelwood rate form is

$$\ln\left(\frac{C_0}{C}\right) = \frac{t}{\tau} \tag{2}$$

where $C$ is the concentration of the reactant (ppm), $C_0$ the initial concentration of the reactant (ppm), $t$ the irradiation time (s) and $\tau$ is the constant of photocatalytic activity. According to Eq. (2), the smaller of the $\tau$ value the better of the photocatalytic activity of the coatings.

## 3. Results and discussion

### 3.1. Heat-treated $TiO_2$ and composite $TiO_2$–$Fe_3O_4$ powders

Fig. 2 shows the X-ray diffraction results of $TiO_2$ and $TiO_2$–$Fe_3O_4$ feedstock powders heat treated at various temperatures. At 973 K, anatase $TiO_2$ kept its crystal structure, but magnetite ($Fe_3O_4$) additive disappeared and $Fe_2O_3$ formed consequently (Eq. (3)). At 1123 K, one part of anatase $TiO_2$ transformed into rutile in composite $TiO_2$–$Fe_3O_4$ powders, which did not take place for pure anatase $TiO_2$ powder (Fig. 2(B) a). This implies that the addition of $Fe_3O_4$ improved the anatase–rutile transformation of $TiO_2$–$Fe_3O_4$ powders and the transformation temperature, which was in the range of 973–1123 K, decreased at least 50 K comparing with pure $TiO_2$ powder of 1173 K.

At the heat-treated temperature of 1273 K, anatase phase transformed completely to rutile in composite $TiO_2$–$Fe_3O_4$ powders. But anatase $TiO_2$ phase was still detectable in pure $TiO_2$ powder. At the higher temperature of 1423 K, all $Fe_2O_3$ reacted with $TiO_2$ and produced stable $Fe_2TiO_5$ (Eq. (4)):

$$4Fe_3O_4 + O_2 \rightarrow 6Fe_2O_3 \tag{3}$$

$$Fe_2O_3 + TiO_2 \rightarrow Fe_2TiO_5 \tag{4}$$

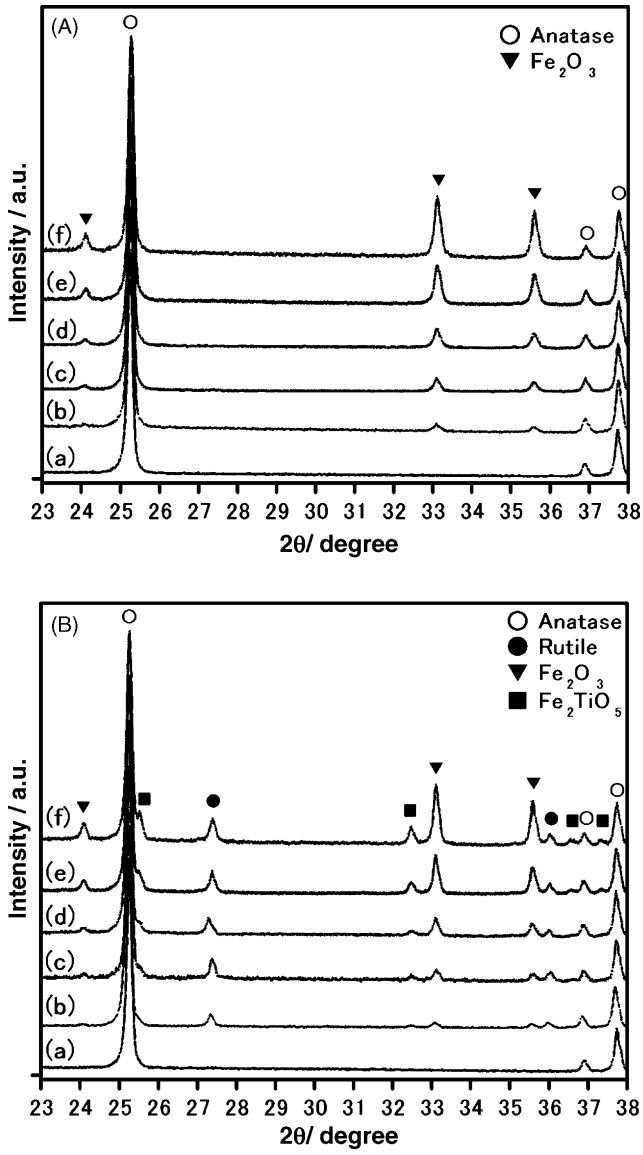


Fig. 2. X-ray diffraction patterns of heat-treated $TiO_2$ and $TiO_2$–$Fe_3O_4$ feedstock powders at 973 K (A) and 1123 K (B) (Notes: (a) $TiO_2$ powder, (b) $TiO_2$–5%$Fe_3O_4$ powder, (c) $TiO_2$–10%$Fe_3O_4$ powder, (d) $TiO_2$–12.7%$Fe_3O_4$ powder, (e) $TiO_2$–22.5%$Fe_3O_4$ powder and (f) $TiO_2$–32.6%$Fe_3O_4$ powder.)

### 3.2. Compositions of plasma-sprayed $TiO_2$ and $TiO_2$–$Fe_3O_4$ coatings

The X-ray diffraction patterns of plasma-sprayed $TiO_2$ and $TiO_2$–$Fe_3O_4$ coatings are illustrated in Fig. 3. The relative intensity of anatase phase decreased with the increasing of $Fe_3O_4$ amount, which indicates that the feedstock powders were more melted with the addition of $Fe_3O_4$. This was in good agreement with the results of heat-treated feedstock powders discussed in Section 3.1. $FeTiO_3$ phase appeared with the addition of $Fe_3O_4$ till 22.5% (Eq. (5)), and became undetectable with the additive amount to 32.6%. The relative intensity of $FeTiO_3$ was highest in $TiO_2$–10%$Fe_3O_4$ coating comparing with the other coatings, which indicates that this coating had the highest content of $FeTiO_3$ compound. However, $FeTiO_3$ phase, which is thermally metastable compound, did not appear in heat-treated

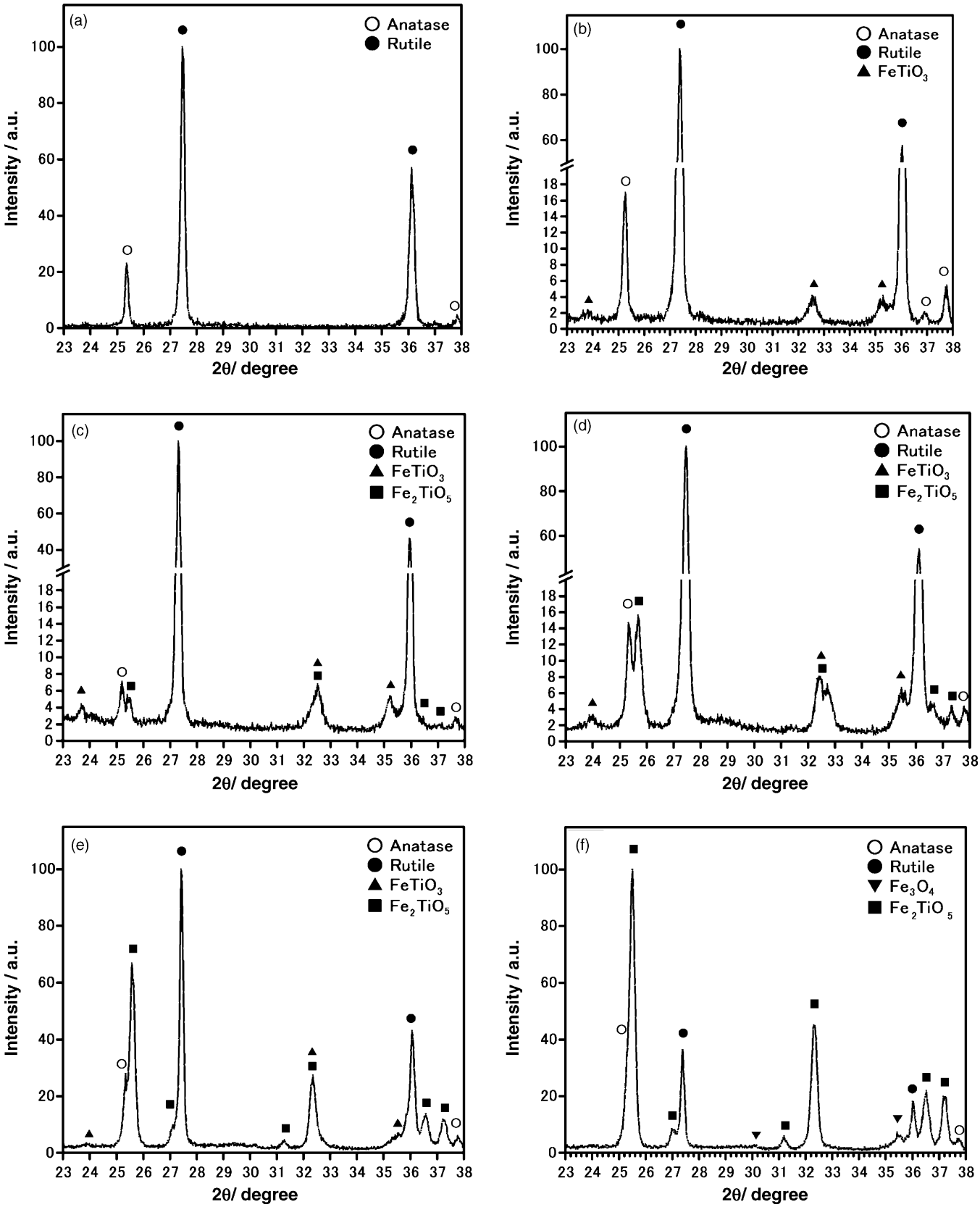


Fig. 3. X-ray diffraction patterns of $TiO_2$ and $TiO_2$–$Fe_3O_4$ coatings plasma sprayed under the arc current of 400 A and spraying distance of 70 mm: (a) $TiO_2$ coating, (b) $TiO_2$–5%$Fe_3O_4$ coating, (c) $TiO_2$–10%$Fe_3O_4$ coating, (d) $TiO_2$–12.7%$Fe_3O_4$ coating, (e) $TiO_2$–22.5%$Fe_3O_4$ coating and (f) $TiO_2$–32.6%$Fe_3O_4$ coating.

$TiO_2$–$Fe_3O_4$ powders. Thus, it can be inferred plasma-spraying technique is a method to form metastable substance:

$$Fe_3O_4 + 2TiO_2 \rightarrow FeTiO_3 + Fe_2TiO_5 \quad (5)$$

The peak intensity of $Fe_2TiO_5$ phase increased continuously and obviously with the increasing of $Fe_3O_4$ amount, and finally became the main phase with the almost complete disappearance of ilmenite $FeTiO_3$ in the sprayed coating. For the high content of $Fe_3O_4$ in the $TiO_2$–32.6%$Fe_3O_4$ powder and high coating formation speed, a few $Fe_3O_4$ remained in the coating.

The formation of $Fe_2TiO_5$ is reported by the fact that certain percentage of $Fe^{3+}$ ion diffuses into $TiO_2$ producing a substitutional solid solution where $Fe^{3+}$ is dispersed in the lattice of $TiO_2$ due to the ion radius similarity of $Fe^{3+}$(0.67 Å) and $Ti^{4+}$(0.64 Å). The substitution of $Fe^{3+}$ in the matrix of $TiO_2$ is a favorable process [32]. This reason resulted in the high amount of $Fe_2TiO_5$ in the sprayed coatings when more anatase $TiO_2$ particles transformed into rutile.

During the short residence time in the plasma jet, the feed particles are completely/partially melted. The droplets impact on a substrate and experience a cooling rate of $10^4$ to $10^6$ K/s, therefore, solid solution, amorphous phase and phase segregation exists widely in composite coating [33,34]. The existence of these kinds of phenomena in sprayed $TiO_2$–32.6%$Fe_3O_4$ coatings was investigated. As clearly shown in Fig. 4, the relative intensity of the main diffraction of rutile phase (1 1 0) increased obviously when the coating was heat treated at 1273 K, and became higher than that of $Fe_2TiO_5$ phase (1 0 1). The ratio of main diffraction intensity of rutile phase (1 1 0) and $Fe_2TiO_5$ phase (1 0 1) of heat-treated $TiO_2$–32.6%$Fe_3O_4$ coating was comparable to that of heat-treated $TiO_2$–32.6%$Fe_3O_4$ powder. The XRD peaks of sprayed $TiO_2$–32.6%$Fe_3O_4$ coatings were not broad, which implies amorphous phase did not exist in it. According to the EDAX analysis results, Ti and Fe elements distributed uniformly along the perpendicular line to the coating surface, which indicates that $TiO_2$ and $Fe_2TiO_5$ phase segregations did not happen. It was confirmed again that Fe/(Ti + Fe) in the sprayed coating was comparable to that in $TiO_2$–32.6%$Fe_3O_4$ feedstock powder. As shown in Fig. 4(b), large amount of Ti segregated from $TiO_2$ and/or $Fe_2TiO_5$ phase after heat treatment of coating, and then the weight fraction of $TiO_2$ increased obviously. Therefore, it is considered that solid solution existed in the sprayed $TiO_2$–32.6%$Fe_3O_4$ coating.

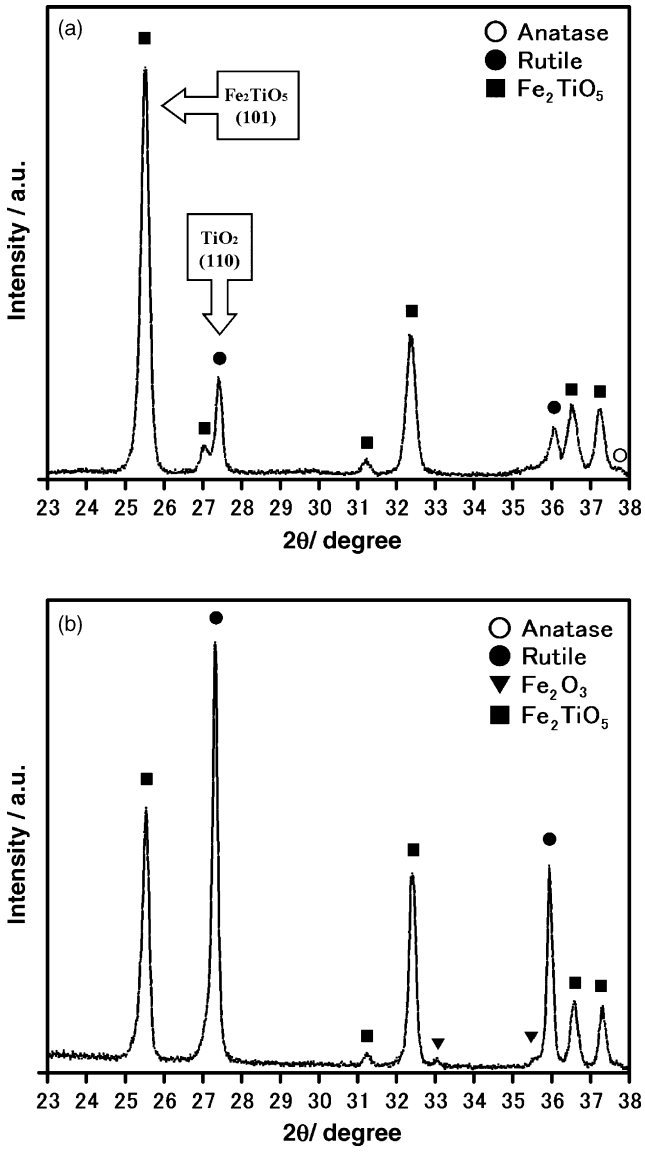


Fig. 4. Phase changes after heat treatment of $TiO_2$–32.6%$Fe_3O_4$ coating prepared under the arc current of 600 A: (a) original coating and (b) heat treated at 1273 K of (a).

### 3.3. Energy absorbance of feedstock powders and sprayed coatings

The photocatalytic performance is affected by catalyst substance, light absorptive ability, morphology, surface active site and so on. Because the light absorptive ability of the photocatalyst is a main factor to affect the photocatalytic activity, the diffuse reflectance of feedstock powders, sprayed $TiO_2$ and $TiO_2$–$Fe_3O_4$ coatings was investigated using the Shimadzu UV-3100PC scanning spectrophotometer. Generally, the photocatalytic activity increases with the increase of light absorptive capacity [26].

According to the diffuse reflectance spectra of the feedstock powders (Fig. 5), the $Fe_3O_4$ additive did not change the absorption edge (wavelength coordinate of black circle in Fig. 5) and the light absorbance drops suddenly in the wavelength range of 340–400 nm. These imply that $Fe_3O_4$ particle cannot shift the photo-absorptive ability of $TiO_2$ to the visible spectral range. The diffuse reflectance spectra of the sprayed coatings are shown in Fig. 6, and to investigate the absorptive relation between light source used in this study and the sprayed coating, the spectral power distribution for UV–lamp is also illustrated in it. The light absorbance of the $TiO_2$ coating dropped suddenly in the wavelength range of 340–400 nm. However, the line slope decreased continuously and the optical absorption edge (black circle) shifted to longer wavelength with the content increase of $Fe_3O_4$ additive. To compare the light absorptive capacity, the integrated energy absorbance of the sprayed $TiO_2$ and $TiO_2$–$Fe_3O_4$ coat-

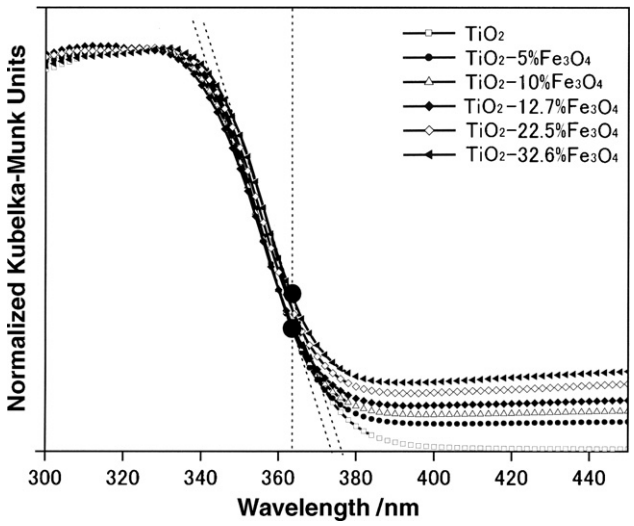


Fig. 5. The diffuse reflectance spectra of the feedstock $TiO_2$ and $TiO_2$–$Fe_3O_4$ powders.

ings from the ultraviolet lamp used in this study was estimated according to Eq. (1). As shown in Fig. 7, the relative integrated energy absorbance increased with the content increase of the $Fe_3O_4$ additive, which means that more irradiation light energy can be utilized. It partly ascribed to $FeTiO_3$ and $Fe_2TiO_5$ compound as reported by Pal et al. [32], Smirnova et al. [35] and Ye [11].

### 3.4. Photocatalytic activity of plasma-sprayed $TiO_2$ and $TiO_2$–$Fe_3O_4$ coatings

Fig. 8(a) illustrates the decomposition characteristic of the acetaldehyde by the sprayed $TiO_2$ and $TiO_2$–$Fe_3O_4$ coatings. It indicates that the plasma-sprayed coatings can decompose acetaldehyde under illumination by ultraviolet rays and the photocatalytic activity of $TiO_2$–10%$Fe_3O_4$ coating was better than that of the other coatings. According to the Eq. (2), the $\tau$ values

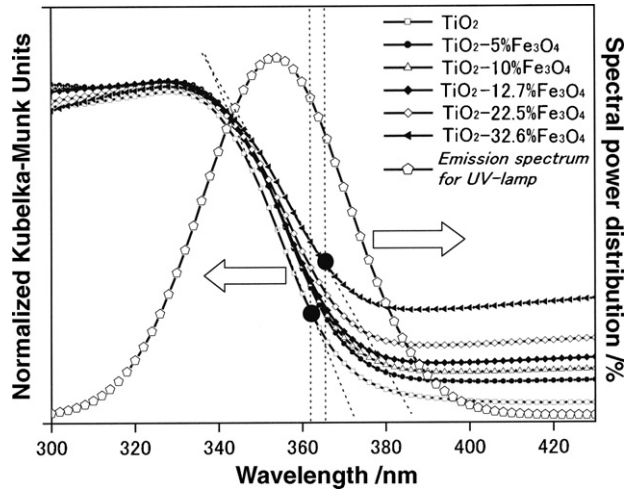


Fig. 6. The diffuse reflectance spectra of the sprayed $TiO_2$, $TiO_2$–$Fe_3O_4$ coatings and the spectral power distribution for the ultraviolet lamp used in this study.

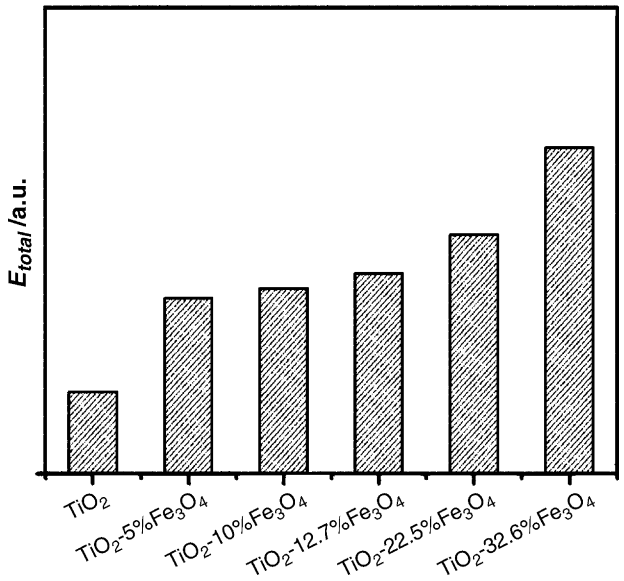


Fig. 7. The integrated energy absorbance of the sprayed $TiO_2$ and $TiO_2$–$Fe_3O_4$ coatings from the ultraviolet lamp used in this study.

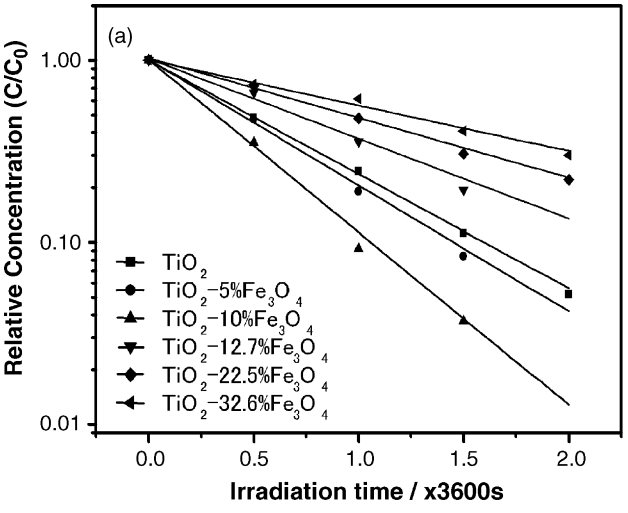


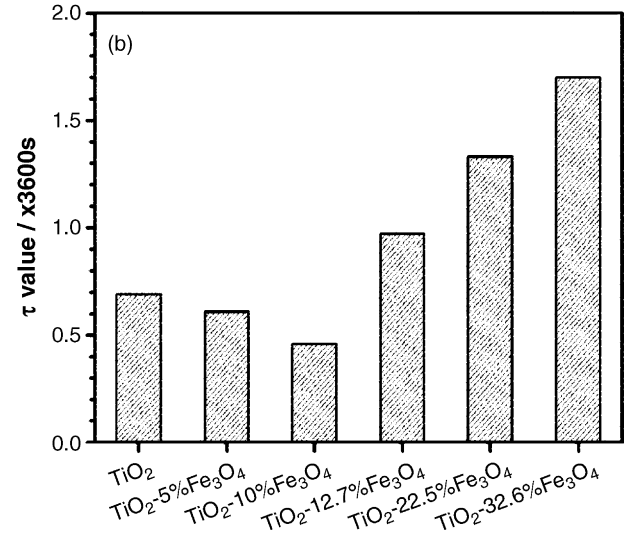


Fig. 8. Photocatalytic decomposition characteristics (a) and $\tau$ values (b) of the sprayed $TiO_2$ and $TiO_2$–$Fe_3O_4$ coatings.

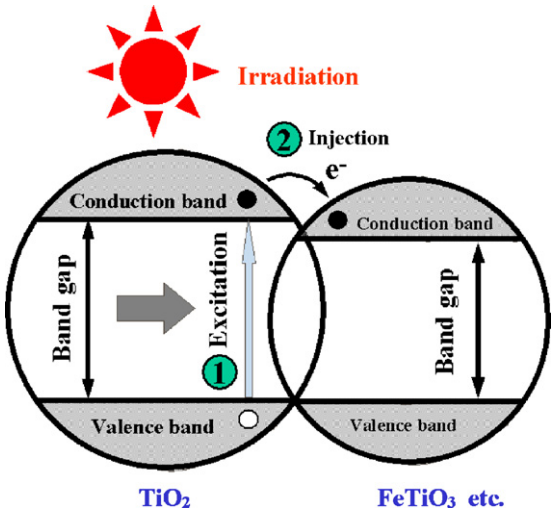


Fig. 9. A proposed two-step electron transfer model for the good photocatalytic activity of $TiO_2$–10%$Fe_3O_4$ coating.

of the sprayed $TiO_2$ and $TiO_2$–$Fe_3O_4$ coatings were calculated as shown in Fig. 8(b). The photocatalytic activity increased with the increasing of $Fe_3O_4$ weight to 10% first, but then decreased.

As discussed in coating composition section, the amount of $FeTiO_3$ phase in the sprayed $TiO_2$–10%$Fe_3O_4$ coating was highest, and the content of $Fe_2TiO_5$ phase increased substantially when the amount of $Fe_3O_4$ additive was over 12.7%. The good photocatalytic efficiency of $TiO_2$–10%$Fe_3O_4$ coating possibly resulted from the high content of ilmenite $FeTiO_3$ phase in the coating, because $FeTiO_3$ has good light absorbance and favorable photo-excited electron–hole separation characters [11]. Furthermore, the band gap of bulk $FeTiO_3$, which is 2.85 eV [36], is lower than that of $TiO_2$. Scaife [37] summarized the findings of some oxide semiconductors including $FeTiO_3$ on the flat band potential, band gaps and stabilities, and the findings indicate the valence band edge of $FeTiO_3$ is about in the same level with that of $TiO_2$. As a possible phenomenon shown in Fig. 9, when the semiconductor is irradiated, the electron possibly transfers (moves) to conduction band in two steps: first step: the electron is initiated from the valence band to the conduction band of $TiO_2$ and second step: the electron in the conduction band of $TiO_2$ injects to the conduction band of $FeTiO_3$. For this two-step mechanism, the lifetime of excited hole and electron pair was prolonged. Perhaps the improved efficiency of the photon is another reason for the good photocatalytic activity of the $TiO_2$–10%$Fe_3O_4$ coatings.

The band gap of pure $Fe_2TiO_5$ is 2.18 eV [38], which is much lower than that of $TiO_2$ and $FeTiO_3$. Although the light absorbance increased with the amount increasing of $Fe_2TiO_5$ compound, the photocatalytic activity was reduced dramatically when the content of $Fe_2TiO_5$ was high. As it is known [32], this kind of phenomenon may result from the unfavorable charge transfer process to adsorbed substance during light illumination where excess accumulation of electron and hole undergoes recombination immediately without taking part in the photocatalytic reaction. Therefore, the electron–hole pair formation and separation process is a key factor in photocatalytic reaction.

As a result, the photocatalytic efficiency of sprayed $TiO_2$–$Fe_3O_4$ coating was improved with an increase of $FeTiO_3$ content in the sprayed coatings. However, when the content of $Fe_3O_4$ additive was over 10%, photocatalytic activity was reduced to large extent due to the presence of large amount of inactive $Fe_2TiO_5$ compound in the $TiO_2$–$Fe_3O_4$ coatings.

## 4. Conclusions

$TiO_2$ and $TiO_2$–$Fe_3O_4$ coatings were prepared on stainless steel substrate by plasma spraying. The results showed that the anatase–rutile transformation temperature of $TiO_2$–$Fe_3O_4$ powders was in the range of 973–1123 K, which was at least 50 K lower than that of pure anatase $TiO_2$ powder. The $TiO_2$–$Fe_3O_4$ coatings consisted of anatase $TiO_2$, rutile $TiO_2$ and pseudobrookite $Fe_2TiO_5$ phase which appeared when the content of $Fe_3O_4$ additive was equal to or over 10%. With relative low amount addition of $Fe_3O_4$, ilmenite $FeTiO_3$ phase existed in the sprayed coatings. The content of anatase $TiO_2$ in the sprayed coatings decreased with the increasing of $Fe_3O_4$ content. The photocatalytic activity was improved with an increase of $FeTiO_3$ content in the coating, which was explained by the good photoabsorbance capacity and by the two-step electron transfer model. However, the presence of large amount of $Fe_2TiO_5$ compound substantially reduced the photocatalytic efficiency of the sprayed $TiO_2$–$Fe_3O_4$ coatings for the unfavorable electron–hole transfer process.

## Acknowledgement

This work was supported by the Scientific Research Foundation for the Returned Overseas Chinese Scholars, Tianjin.

## References

[1] A. Fujishima, K. Honda, Nature 238 (1972) 37–38.
[2] A. Fujishima, T.N. Rao, D.A. Tryk, J. Photochem. Photobiol. C: Photochem. Rev. 1 (2000) 1–21.
[3] J.A. Navío, G. Colón, M. Macías, P.J. Sánchez-Soto, V. Augugliaro, L. Palmisano, J. Mol. Catal. A: Chem. 109 (1996) 239–248.
[4] J.A. Navio, G. Colon, J.M. Herrmann, J. Photochem. Photobiol. A 108 (1997) 179–185.
[5] L. Bahadur, N.R. Tata, J. Photochem. Photobiol. A 91 (1995) 233–240.
[6] M.R. Dhananjeyan, V. Kandavelu, R. Renganathan, J. Mol. Catal. A: Chem. 151 (2000) 217–223.
[7] B. Pal, T. Hata, K. Goto, G. Nogami, J. Mol. Catal. A: Chem. 169 (2001) 147–155.
[8] A.K.G. Carlos, F. Wypych, S.G. Moraes, N. Duran, N. Nagata, P. Peralta-Zamora, Chemosphere 40 (2000) 433–440.
[9] B. Neppolian, H.C. Choi, S. Sakthivel, B. Arabindoo, V. Murugesan, J. Hazard. Mater. 89 (2002) 303–317.
[10] L. Bayer, I. Eroglu, L. Turker, Sol. Energy Mater. Sol. Cells 62 (2000) 43–49.
[11] F.X. Ye, A. Ohmori, Surf. Coat. Technol. 160 (2002) 62–67.
[12] P. Calza, C. Minero, A. Hiskia, Appl. Catal. B: Environ. 21 (3) (1999) 191–202.
[13] A. Mills, J. Wang, J. Photochem. Photobiol. A 127 (1999) 123–134.
[14] K. Tennakone, U.S. Ketipearachchi, Appl. Catal. B: Environ. 5 (1995) 343–349.

[15] F. Zhang, J. Zhao, T. Shen, H. Hidaka, E. Pelizzetti, N. Serpone, Appl. Catal. B: Environ. 15 (1998) 147–156.
[16] A. Sclafani, J. Herrmann, J. Photochem. Photobiol. A 113 (2) (1998) 181–188.
[17] Z. Ilisz, A. Laszlo, Dombi, Appl. Catal. A: Gen. 180 (1999) 25–33.
[18] Y. Lee, T. Watanabe, T. Takata, M. Hara, M. Yoshimura, K. Domen, Bull. Chem. Soc. Jpn. 80 (2007) 423–428.
[19] A. Kudo, K. Domen, K. Maruya, T. Onishi, Chem. Phys. Lett. 133 (1987) 517–551.
[20] K. Maeda, N. Saito, D. Lu, Y. Inoue, K. Domen, J. Phys. Chem. C 111 (2007) 4749–4755.
[21] T. Ishii, H. Kato, A. Kudo, J. Photochem. Photobiol. A 163 (2004) 181–186.
[22] R. Asahi, T. Morikawa, T. Ohwaki, K. Aoki, Y. Taga, Science 293 (2001) 269–271.
[23] J.-F. Zhu, W. Zheng, B. He, J.-L. Zhang, M. Anpo, J. Mol. Catal. A: Chem. 216 (2004) 35–43.
[24] H. Yamashita, M. Harada, J. Misaka, M. Takeuchi, B. Neppolian, M. Anpo, Catal. Today 84 (2003) 191–196.
[25] C.-J. Li, A. Ohmori, J. Therm. Spray Technol. 11 (2002) 365–374.
[26] Z. Zou, J. Ye, K. Sayama, H. Arakawa, Chem. Phys. Lett. 343 (2001) 303–308.
[27] P.D. Fochs, Proc. Phys. Soc. B69 (1956) 70–75.
[28] S.P. Tandon, J.P. Gupta, Phys. Stat. Sol. 38 (1970) 363–367.
[29] I. Sopyan, M. Watanabe, S. Murasawa, K. Hashimoto, A. Fujishima, J. Photochem. Photobiol. A 98 (1996) 79–86.
[30] A.V. Vorontsov, A.A. Altynnikov, J. Photochem. Photobiol. A 144 (2001) 193–196.
[31] P.H. Chen, C.H. Jenq, Environ. Int. 24 (8) (1998) 871–879.
[32] B. Pal, M. Sharon, G. Nogami, Mater. Chem. Phys. 59 (1999) 254–261.
[33] P. Bansal, N.P. Padture, A. Vasiliev, Acta Mater. 51 (2003) 2959–2970.
[34] Y.Z. Yang, Z.G. Liu, Z.Y. Liu, Y.Z. Chuang, Thin Solid Films 388 (2001) 208–212.
[35] N. Smirnova, A. Eremenko, O. Rusina, W. Hopp, L. Spanhel, J. Sol–Gel Sci. Technol. 22 (1/2) (2001) 109–113.
[36] M.A. Butler, D.S. Ginley, Chem. Phys. Lett. 47 (2) (1977) 319–321.
[37] D.E. Scaife, Sol. Energy 25 (1980) 41–54.
[38] D.S. Ginley, M.A. Butler, J. Appl. Phys. 48 (5) (1977) 1021–2019.